Journal of Energy Storage 55 (2022) 105628

Contents lists available at ScienceDirect

Journal of Energy Storage

journal homepage: www.elsevier.com/locate/est

Research papers

Triethylammonium thiocyanate ionic liquid electrolyte-based supercapacitor fabricated using coconut shell-derived electronically conducting activated charcoal electrode material

A.D.T. Medagedara [a,b], N.M. Waduge [a,c], T.M.W.J. Bandara [b,d], I.G.K.J. Wimalasena [a,b], M. Dissanayake [a,b], K. Tennakone [a,e], R.M.G. Rajapakse [b,f], C.P. Rupasinghe [c], G.R.A. Kumara [a,*]

[a] National Institute of Fundamental Studies, Hantana Road, Kandy, Sri Lanka
[b] Postgraduate Institute of Science, University of Peradeniya, Sri Lanka
[c] Department of Agriculture Engineering, University of Ruhuna, Kaburupitiya, Sri Lanka
[d] Department of Physics, University of Peradeniya, Peradeniya, Sri Lanka
[e] Department of Physics, Georgia State University, Atlanta, USA
[f] Department of Chemistry, University of Peradeniya, Peradeniya, Sri Lanka

ARTICLE INFO

Keywords:
Activated carbon
Supercapacitor
Triethylammonium thiocyanate
Ionic liquid electrolyte

ABSTRACT

Organic solvents are commonly used as commercial electrolytes in supercapacitors, but they have several drawbacks, such as high volatility, toxicity, and environmental issues. To overcome these problems, ionic liquids are used though their high costs hamper commercial applications. In this study, a novel and low-cost ionic liquid based on triethylammonium cation and thiocyanate anion were synthesized and used as the electrolyte in a low-cost supercapacitor fabricated using electronically conducting activated carbon derived from cleaned coconut shells as electrode material. The temperature dependence of electrolyte conductivity was investigated, in the frequency range of 1 Hz-500 kHz, using AC impedance analysis, in the temperature range from 30 °C - 90 °C in ten-degree increments and found to be in the range of 4.5 to 14.4 mS cm^{-1}. The ion transport kinetics behaves according to the Vogel-Tammann-Fulcher (VTF) model with an activation energy (E_a) and the pre-exponential factor ($A_{\sigma T}$) of 0.0158 eV and 114.9 S m^{-1} $K^{1/2}$, respectively. The activated carbon material developed has a high porosity and high electronic conductivity. The electrode fabrication methodology was optimized by varying the polyvinylpyrrolidone (PVP) binder amount with respect to the mass of activated carbon on a titanium sheet as a function of heat treatment temperature. The supercapacitor that gives the highest specific capacitance is based on the electrode constructed using 5 % *w*/w PVP in 0.50 g of activated carbon deposited on a titanium sheet by heat treating at 200 °C for 20 min. At the scan rate of 5 mV s^{-1}, two-electrode CV studies revealed a specific capacitance of 36.8 F g^{-1} for the optimized supercapacitor assembly. The electrolyte triethylammonium thiocyanate (TAT) demonstrated good electrochemical stability and a large operating voltage window of 1.8 V and high stability, with 94.4 % capacity retention after 1000 cycles. The AC impedance studies also gave comparable results.

Prime novelty statement: The manuscript describes a method to prepare a novel and low-cost ionic liquid material triethylammoniumthiocyanate starting from triethylamine and ammonium thiocyanate, and its application as the ionic liquid electrolyte in a low-cost supercapacitor. The electrode material used in the supercapacitor was fabricated using electronically conducting activated carbon derived from cleaned coconut shells, which were deposited firmly adhering to titanium sheets using polyvinylpyrrolidone binder under optimized heat treatment conditions. As such, both the ionic liquid electrolyte and the activated carbon electrode material are novel and attractive materials for the commercial production of low-cost supercapacitors.

* Corresponding author at: National Institute of Fundamental Studies, Hantana Road, Kandy, Sri Lanka.
E-mail address: grakumara2000@yahoo.com (G.R.A. Kumara).

https://doi.org/10.1016/j.est.2022.105628
Received 11 March 2022; Received in revised form 10 August 2022; Accepted 3 September 2022

1. Introduction

The whole world is gradually moving into renewable power sources due to the depletion of fossil fuel resources and adverse environmental effects associated with their usage [1]. As such, novel, cost-effective, and highly efficient electrochemical power sources, such as secondary batteries, fuel cells, and supercapacitors are to be developed to make use of renewable energy in a more effective manner [2,3]. Supercapacitors can be identified as a promising alternative to secondary batteries and conventional capacitors.

This consists of two strategies for storing energy, namely, static double-layer capacitance and electrical pseudo-capacitance [4,5]. Supercapacitors have higher capacitance values than standard capacitors and higher power densities and lower energy densities when compared to those of batteries [6]. Supercapacitors typically require a very short charging time compared to that of secondary batteries, and they have a significantly large number of life cycles along with high capacitance retention, which are the characteristics of a good power source [7]. A recent study found that a unique quasi-solid-state supercapacitor maintained 98.6 % of its capacity after 50,000 cycles [8]. As a result, improving supercapacitor performance and reducing their cost of production can have a significant impact on future energy storage technologies.

Several factors influence the performance of a supercapacitor; most notably the type and the nature of electrode material, separator, electrolytes, and binders used to fabricate the electrode [9–12]. When it comes to activated carbon-based supercapacitors, the process of activation can have an impact on their performance [13]. The synthesis method of the electrode plays a crucial role when it comes to the structural and electrochemical properties of the supercapacitor. In recent studies electrode synthesis methods such as, electropolymerization (electro-deposition), direct coating, chemical vapor deposition (CVD), vacuum filtration, and hydrothermal/solvothermal technique have been commonly used. They have shown a significant improvement in the structural and electrochemical properties of supercapacitors [14–17].

The use of a suitable electrolyte has a significant impact on supercapacitor performance. Aqueous electrolytes have several significant disadvantages, and one such drawback is their low operating voltage windows (OPWs) [18]. This problem can be circumvented by using an organic electrolyte, gel polymer electrolyte, or an ionic liquid electrolyte [8,19,20]. In particular, ionic liquids have impressively broad OPWs. When a supercapacitor is made with these electrolytes, the device's maximum operating potential window (OPW) is always less than the expected voltage stability window of the electrolyte. This is especially true for ionic liquid electrolytes, which are stable in the 5–6 V range when platinum electrodes are used, but rarely work beyond 3.5 V in supercapacitors [20]. One of the primary reasons for lower working potentials is parasitic reactions in the cell, which are usually caused by impurities in the electrode material as well as by the electrochemically active surface functional groups [21,22].

The specific energy (E) and power (P) of supercapacitors are defined by $E = \frac{1}{2}CV^2$and $P = \frac{4V^2}{R}$, respectively, where C, V and R are the capacitance, the operative voltage, and the equivalent series resistance (ESR) of the electrochemical double-layer capacitor [23]. The above equations show how voltage influences the energy and power of a supercapacitor. It is, therefore, important to have a large OPW for an electrolyte to attain high voltages and thereby achieve a high energy density and power of a supercapacitor. Since ionic liquids offer relatively large OPW, focusing research on using them will enable to develop supercapacitors with high E and P values [14]. The use of ionic liquid, triethylammonium thiocyanate (TAT), as an electrolyte material for the electrochemical double-layer capacitor (EDLC) is demonstrated in this paper.

Our previous studies used TAT as a crystal growth inhibitor for cuprous iodide hole conductors used in dye-sensitized solid-state solar cells (DSSCs). This enabled pore filling of interconnected TiO_2 nanoparticles to improve the efficiencies of DSSCs [24]. The thiocyanate ion possesses ubiquitous properties. It is readily adsorbed on surfaces, improving pore filling. When alkali metal halides are compared with thiocyanate in aqueous electrolytes of supercapacitors, thiocyanate is found to yield higher capacitance. This has motivated us to examine ionic liquids based on thiocyanate. In addition, the electrode material also has an impact on the supercapacitor's specific capacitance. Carbon-based materials are often used as an electrode material for supercapacitors as well as an anode electrode material for lithium-ion batteries (LIBs) because of their unique thermal, structural and electrochemical properties. In LIBs, a carbon coating functions as an anode material. This has the ability to slow down the deterioration of the active electrode material and the electrolyte. A similar procedure can also be applied to lengthen the life of the supercapacitors [25]. A variety of electrode materials such as carbon nanotubes, graphene, activated carbon, templated porous carbon, functionalized porous carbon, and carbon aerogels were most used [26–31].

There are some reports on using ionic liquids as electrolytes for SC but, to the best of our knowledge, there is no reports in the literature on using TAT in supercapacitor applications. In addition, this innovative study reveals that a relatively high specific capacitance can be achieved by using low-cost carbonaceous electrodes prepared using active carbon derived from coconut shells. Interestingly, this SC can be operated at a voltage window as high as 1.8 V and it exhibits high stability, along with 94.4 % capacity retention after 1000 cycles.

2. Experimental

2.1. Materials used

Coconut shell, which is abundant in Sri Lanka, was used to make activated carbon as an electrode material. As a current collector, titanium plates with dimensions of 2 cm × 1 cm × 0.45 mm (length x width x thickness) were used. Ammonium thiocyanate (NH_4SCN, 98.0 % (m/m) assay) and dichloromethane (CH_2Cl_2, 99.5 % (m/m) assay) were purchased from Fujifilm Wako Pure Chemical Corporation, Osaka, Japan. Triethylamine ($C_6H_{15}N$, 99.0 % purity) was purchased from Daejung Chemicals, Siheung-si, South Korea. Hexane (C_6H_{14}, 99.0 % purity) was procured from Sigma-Aldrich, St. Louis, Missouri, United States. Medium retention filter papers (model-F1001, retention range 10-13 μm) were obtained from Chmlab, Barcelona, Spain.

2.2. Methods

2.2.1. Preparation of the triethylammonium thiocyanate ionic liquid electrolyte

For the preparation of the TAT ionic liquid electrolyte, the mixture of ammonium thiocyanate and triethylamine (triethylamine in 25 % excess of the stoichiometric amount) was slowly heated up to 120 °C on a hotplate under anhydrous conditions and allowed to heat at this temperature for 2–3 min [18]. This has resulted in the formation of TAT with the expelling of ammonia gas, as shown in Eq. (1).

$$(C_2H_5)_3N(l, 25\ \text{mol\%excess})) + NH_4SCN(s, \text{dissolved in trimethylamine}) \xrightarrow{120^{\circ}C} (C_2H_5)_3NH^+(l) + SCN^-(l) + NH_3(g) \quad (1)$$

The reaction shown in Eq. (1) is accelerated by the removal of ammonia from the liquid phase. However, to avoid the condensation of ammonia and moisture and return to the reaction mixture as ammonium hydroxide, it is necessary to maintain strict anhydrous conditions. Therefore, the methyl ammine liquid used was dried with silica gel to remove any water present in it. The NH_4SCN solid used was dried in a vacuum oven at 60 °C for 24 h to make sure that it was also anhydrous.

The anhydrous NH_4SCN was then dissolved in $(C_2H_5)_3N$ liquid in 1: 1.25 M ratio and heated slowly, under anhydrous conditions, until the temperature reaches 120 °C, at which the heating continued for 2–5 min. Then, the above reaction takes place and $(C_2H_5)_3NH^+$(l) and SCN^-(l) ions separate from the remaining reaction mixture as the ions are not soluble in $(C_2H_5)_3N$. Since the ionic fraction is the heaviest, it separates out to the bottom of the reaction vessel. The ionic component and some unreacted $(C_2H_5)_3N$ and NH_4SCN were then separated using a separating funnel. However, the ionic component still contains some trapped $(C_2H_5)_3N$ and NH_4SCN. The product was then washed repeatedly with hexane to remove excess $(C_2H_5)_3N$. The ionic component was dissolved in dichloromethane and any unreacted NH_4SCN was separated by centrifugation. The colorless and transparent ionic liquid of $(C_2H_5)_3NH^+$(l) + SCN^-(l)was obtained by evaporating dichloromethane, which was subsequently dried under vacuum, at 70 °C, for 1 h, and subsequently at 30 °C for 5 days [32].

Electrochemical impedance spectroscopy (EIS) was used to determine the characteristics of the TAT electrolyte, at different temperatures from 30 °C to 90 °C, in ten-degree increments, in the frequency range 1 Hz-500 kHz. The TAT ionic liquid electrolyte sample was sandwiched between two small stainless steel cylinders, placed in a plastic tube as shown in Fig. 1 (a) and placed in an empty beaker. The two stainless steel cylinders were connected to the frequency response analyzer of the Metrohm Autolab Potentiostat/Galvanostat using crocodile clip attached copper wires. The whole setup was then placed in an oil bath placed on a hot plate, and EIS measurements were performed at different temperatures in the range from room temperature to 90 °C (Fig. 1 (b)). For each measurement, the temperature of the sample was allowed to stabilize for 10 min.

2.2.2. *Activated carbon and suspensions of activated carbon*

The activated carbon was prepared starting from coconut shells. To

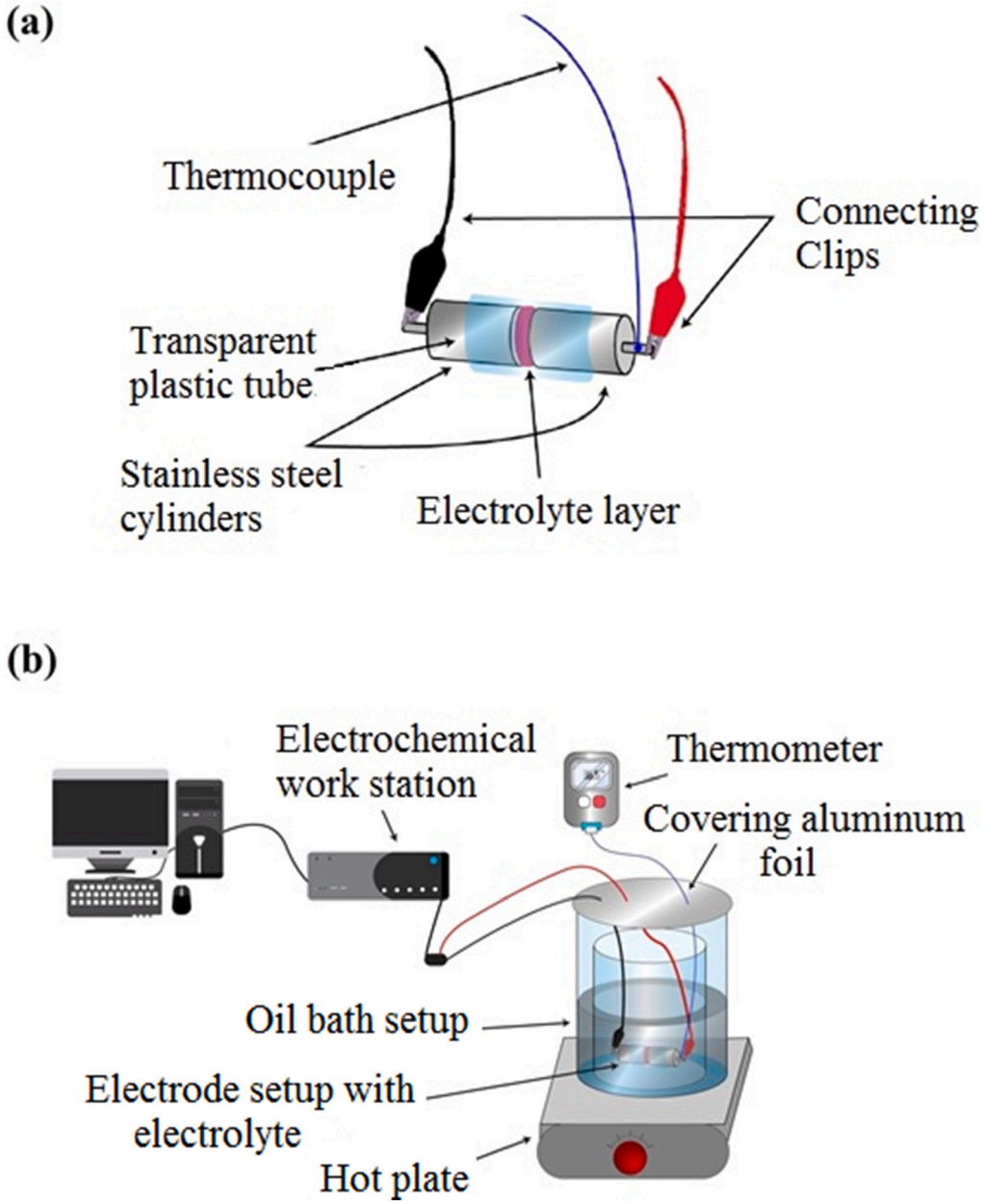

Fig. 1. (a) A schematic representation of the cell made by sandwiching the trimethylammonium thiocyanate ionic liquid electrolyte between two stainless steel cylinders which were placed in a plastic tube. (b) The set up used to measure electrochemical impedance data of the trimethylammonium thiocyanate ionic liquid electrolyte at different temperatures.

do so, the coconut shells were cleaned by scraping away their fibrous materials. The cleaned coconut shells were burned in a metal chamber until the flames emitted from the volatile matter became incandescent. The burnt coconut shells were quenched by putting them into distilled water. They were then heated, at 900 °C, for 20 min, in a box furnace. The hot charcoal thus obtained was put into a distilled water tank to quench it again and cool it down. They were then removed from the tank, dried, and ground into a powder [13]. The grinding process was continued for 10 min to obtain a fine powder sample, and a disc mill was used in this step. A schematic diagram along with relevant photographic images to illustrate the process of making activated carbon powder from coconut shells is given in Fig. 2. The resulted samples were characterized by X-ray diffraction (XRD; RigakuUltima IV X-ray powder diffractometer), nitrogen adsorption measurements (Micromeritics 3Flex surface characterization analyzer) and scanning electron microscopy (SEM-SU6600 12.0 kV SEM).

The activated carbon and polyvinylpyrrolidone (PVP) suspensions were prepared as follows. First, suspensions of activated carbon and polyvinylpyrrolidone (PVP) in isopropanol were prepared. To do so, PVP samples of 0.01 g, 0.025 g, 0.035 g, 0.05 g, and 0.75 g were mixed with isopropanol (10.0 ml separately in a quartz mortar for 1–2 min with a pestle). The activated charcoal (0.5 g) was then added to each sample and stirred for a further 3 min to obtain the activated carbon with PVP binder suspensions.

2.3. Fabrication of supercapacitors and characterization

Initially, the titanium current collector plates were cleaned by ethanol, rinsed with de-ionized water, and dried in hot air. Then, cleaned and dried plates were kept on the hot plate at 150 °C for 10 min before spraying the suspension. Fig. 3. (a) shows a photograph of the suspension prepared by dispersing activated carbon and polyvinylpyrrolidone (PVP) in isopropanol. Next, the activated charcoal in PVP suspensions was sprayed separately onto the titanium current collector plates using the spray coating process. The spray coating was accomplished using a spray gun with a nozzle diameter of 1.5 mm. The electrodes thus fabricated were then sintered in a furnace, at 300 °C, for 20 min. Fig. 3(b) shows the electrodes fabricated. The electrodes were wetted with the TAT ionic liquid electrolyte and separated by the membrane so that both surfaces of the membrane are in contact with the electrolyte.

The supercapacitors were then assembled using TAT ionic liquid electrolyte sandwiched between the two electrodes, where the assembly of the different components is schematically illustrated in Fig. 3(c). The two current collector electrodes were then connected to the Metrohm Autolab Potentiostat/Galvanostat and the cyclic voltammograms (CVs) were recorded at 5, 10, and 15 mV s^{-1} potential scan rates in the potential range from 0 V to +1.0 V. EIS was performed using FRA module, and the fitting to the most appropriate equivalent circuit was done using built-in NOVA software. To investigate the cell's open voltage window, CVs were done at 10 mV s^{-1} in various potential ranges ranging from 0 V (lower vertex) to +1.0 V (upper vertex), with the upper vertex increasing by 0.2 V increments. In addition, 1000 CV cycles at a 100 mV s^{-1} scan rate were done to test the cell's cycle life. Before and after 1000 cycles, EIS was done in order to check the losses during the cycling.

A computer-controlled Metrohm Autolab Potentiostat/Galvanostat Electrochemical Analyzer was used to perform the CV, galvanostatic charge/discharge (GCD) curves and EIS measurements. The potential sweep rate was set to 10 mV s^{-1} during CV testing. Eq. (2) was used to calculate the cell capacitance.

$$C = \frac{1 \int IdV}{2m\Delta V \frac{dV}{dt}} \tag{2}$$

where m is the mass of activated carbon layer on the electrode surface, I is the current, ΔV is the potential range used and $\frac{dV}{dt}$ is the potential scan rate used in the CV experiments.

3. Results and discussion

3.1. Characterization of activated carbon

Fig. 4(a) depicts the SEM images of the activated carbon material prepared which indicate particles with different sizes in the micrometer range with high porosity. The P-XRD pattern of the resulting activated charcoal sample shows no sharp diffraction peaks, as would be expected in a highly crystalline material. Due to the very amorphous nature of the charcoal, the peaks are broad. However, it shows two broad peaks at $2\theta = 24.655°$ and 43.705°, which correspond to diffractions from (002) and (100) planes of the activated carbon standard P-XRD pattern (JCPDS 75–1621). There are no other diffraction peaks, indicating that the generated activated charcoal sample is free of crystalline contaminants.

.

In the Raman spectra of activated charcoal, two bands are observed. The band at 1350 cm^{-1} corresponds to the D band, while that at 1600 cm^{-1} corresponds to the G band of activated charcoal [33]. The graphite band (G band) relates to perfect graphitic vibration modes, whereas the defect band (D band) refers to disordered graphite. When the intensities

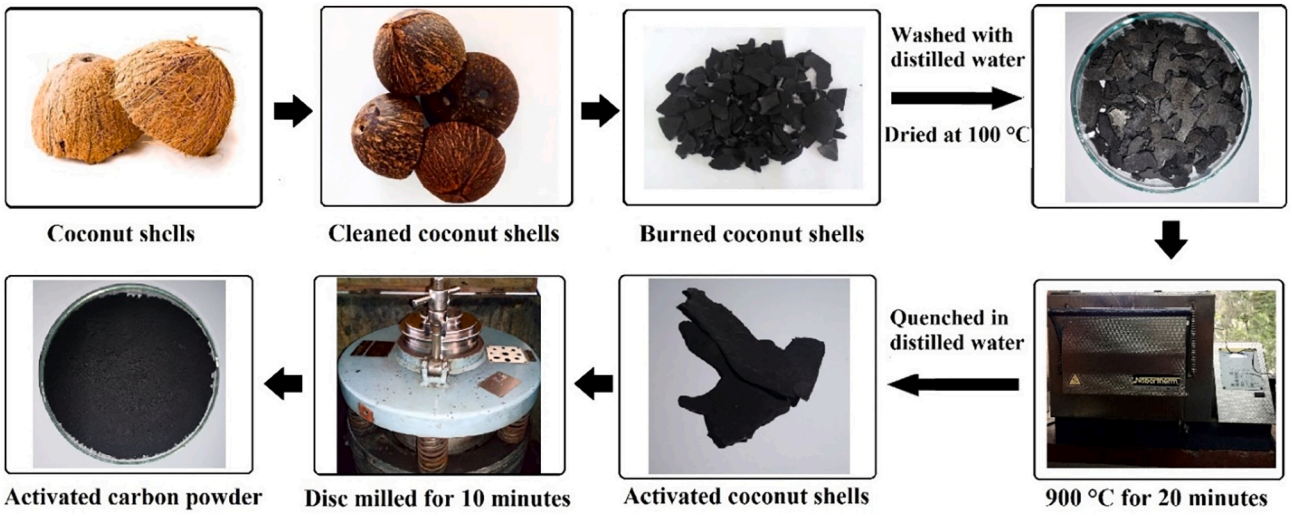

Fig. 2. Schematic diagram of the process of making activated carbon powder from coconut shells.

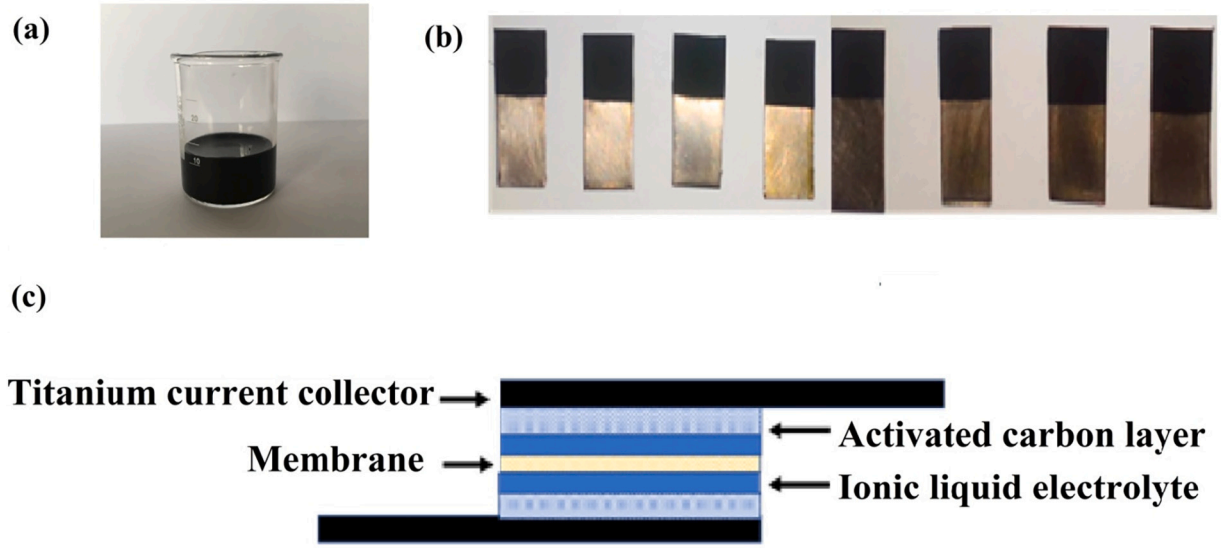

Fig. 3. (a) Photograph of the suspension made by dispersing activated carbon and polyvinylpyrrolidone (PVP) in isopropanol. (b) Titanium current collector plates after depositing activated carbon in polyvinylpyrrolidone suspension by the spray method. (c) Schematic representation of the different layers in the super-capacitor assembly.

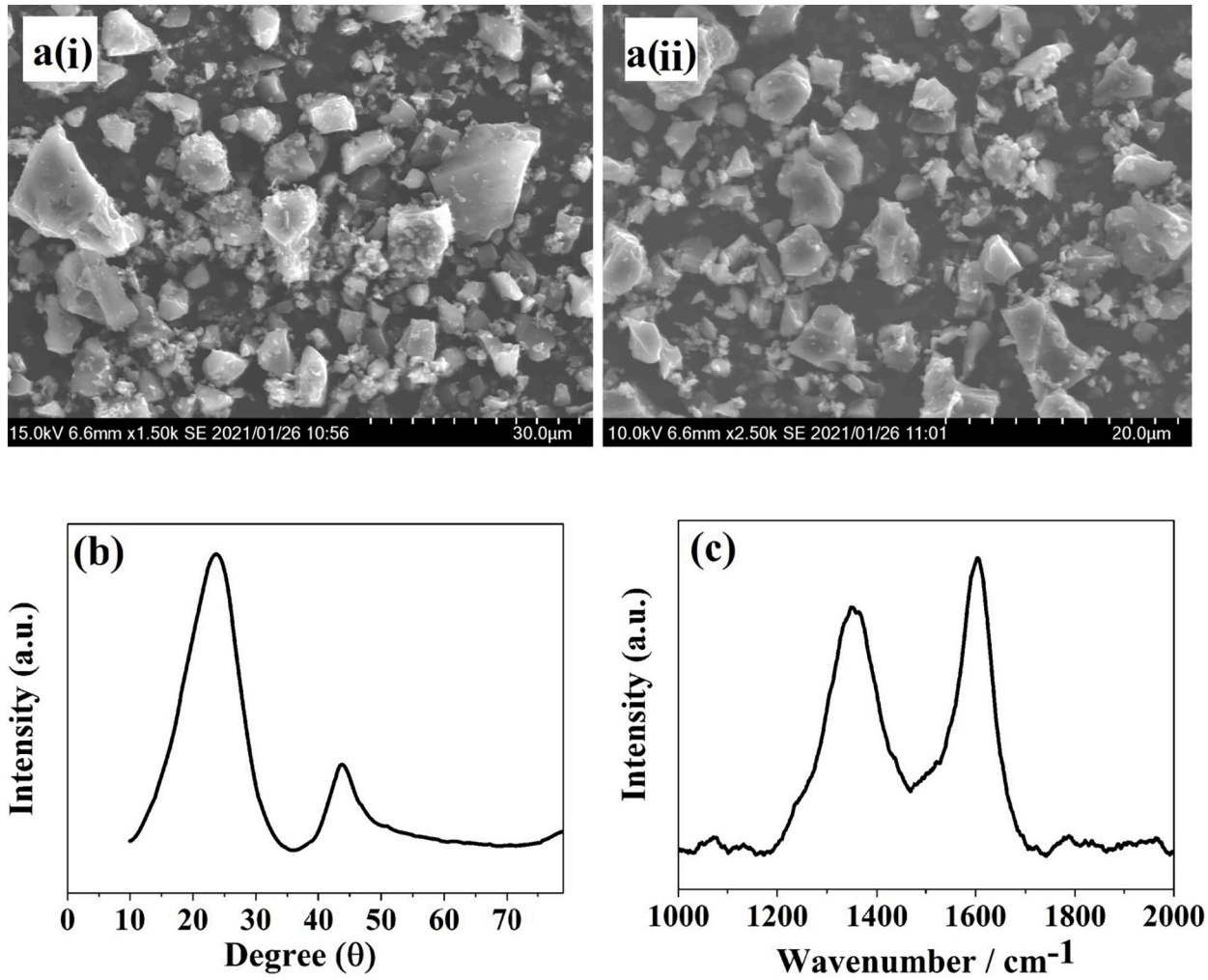

Fig. 4. (a) The SEM images at different magnification levels (i) 1500 (ii) 2500, (b) the powder XRD pattern of activated carbon and (c) the Raman spectrum of activated carbon prepared.

of the two bands are compared, it is possible to conclude that fabricated charcoal contains both graphitic and amorphous carbon, resulting in a larger surface area than pristine graphitic charcoal. This value can be compared with other activated charcoal samples to gain a relative understanding of the disordered degree by taking the ratio of the band peak area (I_D/I_G) [34]. The I_D/I_G value obtained for this sample is 0.83, indicating that this compound has a lesser number of structural defects.

In addition to the above characterizations, the specific surface area and pore characteristics of the activated carbon sample are important to determine the possibility of ion storing capacity of the sample. Nitrogen adsorption-desorption analysis of the activated carbon sample showed Brunauer-Emmett-Teller (BET) surface area and total pore volume, 636 $m^2\ g^{-1}$ and 0.23 $cm^3\ g^{-1}$, respectively.

3.2. Properties of the trimethylammonium thiocyanate ionic liquid electrolyte

Fig. 5 depicts the Nyquist plots of the AC impedance studies of the TAT ionic liquid electrolyte synthesized and used in this work. It is interesting to note that the bulk resistance of the electrolyte decreases as the temperature is increased. This can be due to the increase in ionic mobility since, in general, charge transport kinetics increase with increasing temperature and decrease in local viscosity of the electrolyte as the temperature is increased. Table 1 depicts the bulk resistance data and calculated bulk conductivity data together with resistance for ionic transport data which were determined from the straight-line segment of 45° inclination describing the Warburg impedance portion of the impedance. The ionic conductivity values are in the mS scale, showing sufficient conductivity of the electrolyte for its use in the supercapacitor assembled in this work.

The Eq. (3) describes the variation of the ionic conductivity of an electrolyte as function of temperature [35].

$$\sigma(T) = \frac{A_{\sigma T}\sqrt{T - \left(\frac{\Delta\overline{E}\Delta\overline{Z}}{R}\right)^2}}{T} exp\left(-\frac{\frac{\overline{E}_0\overline{Z}_0}{R}}{T - \frac{\Delta\overline{E}\Delta\overline{Z}}{R}}\right) \quad (3)$$

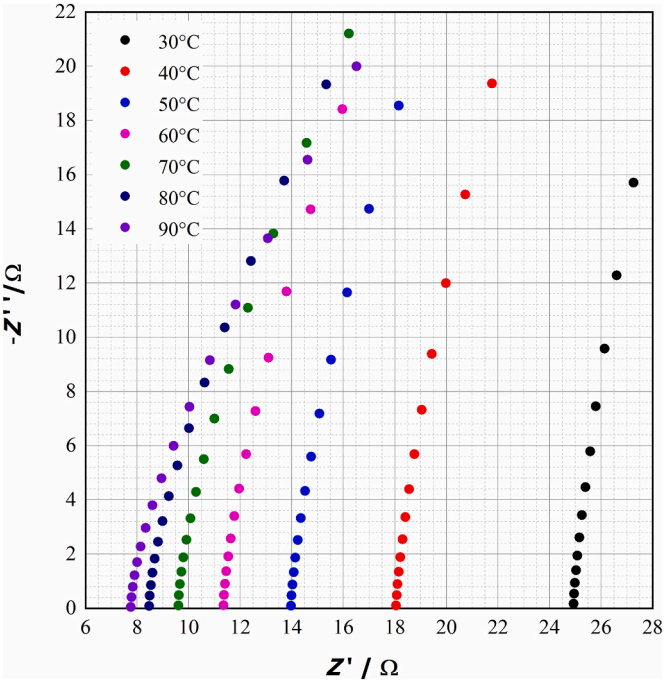

Fig. 5. The Nyquist plots obtained from AC impedance data for the trimethylammonium thiocyanate ionic liquid electrolyte at different temperatures.

Table 1
Temperature dependence of the bulk resistance values and estimated ionic conductivities.

Temperature (°C)	Bulk resistance (Ω)	Ionic conductivity (mS cm^{-1})	Ion transport resistance (Ω)
30	24.92	4.46	95.57
40	18.03	6.17	73.06
50	13.95	7.98	57.35
60	11.33	9.82	50.01
70	9.58	11.61	39.56
80	8.45	13.17	31.35
90	7.74	14.37	24.93

where, $\overline{E}$ is the bond energy between the mobile and the surrounding ion, $\overline{Z}$ is the coordination number of the mobile ion $\overline{E}_0$and $\overline{Z}_0$ are the mean values of $\overline{E}$ and $\overline{Z}$ and $\Delta\overline{E}$ and $\Delta\overline{Z}$ are their fluctuations.T is the absolute temperature, R is the gas constant, $A_{\sigma T}$ is the pre-exponential factor.

Eq. (3) reduces to the Arrhenius-like Eq. (4) when $T \gg \frac{\Delta\overline{E}\Delta\overline{Z}}{R}$.

$$\sigma(T) = A_{\sigma T} exp\left(-\frac{\overline{E}_0\overline{Z}_0}{RT}\right) \quad (4)$$

If Eq. (4) is applicable to the sample, then the plot of $\ln\sigma(T)$ against $\frac{1}{T}$ is a straight-line with $-\frac{\overline{E}_0\overline{Z}_0}{R}$ as its gradient and$\ln(A_{\sigma T})$ as the intercept on the vertical axis.

As shown from Fig. 6 (a), the plot of $\ln\sigma(T)$ against $\frac{1000}{T}$ is not linear and hence the ionic conductivity of the electrolyte does not follow Arrhenius behavior. More sophisticated Equation for the temperature dependence of the ionic conductivity of an electrolyte is given by the Vogel-Tammann-Fulcher (VTF) relationship that is given in Eq. (5).

$$\sigma(T) = A_{\sigma T} T^{-\frac{1}{2}} exp\left[\frac{-E_a}{k_B(T - T_0)}\right] \quad (5)$$

Here, E_a is the pseudo activation energy for ionic transport and T_0 is the ideal glass transition temperature of the electrolyte. The T_0 for trimethylammoniumthiocyanate is 235 K. As can be seen from Fig. 6 (b), the plot of $ln\left(\sqrt{T}\sigma(T)\right)$ against $\frac{1}{(T-T_0)}$is a linear. Therefore the electrolyte obeys the VTF behavior. Then the plot of $ln\left(\sqrt{T}\sigma(T)\right)$ against $\frac{1}{(T-T_0)}$. The activation energy $E_a$and the pre-exponential factor $A_{\sigma T}$is 0.0158 eV and 114.9S m^{-1} $K^{1/2}$, respectively.

3.3. Characterization of supercapacitors fabricated

3.3.1. Optimization of polyvinylpyrrolidone in the preparation of activated carbon suspension

Table 2 shows the specific capacitance of supercapacitors made with 0.50 g of activated carbon and containing different amounts of PVP binder, studied at 300 °C. As revealed by the data, the highest specific capacitance is obtained when the mass of PVP binder used is 5 % of that of activated charcoal. When the binder amount is less than 5 %, the binder used is insufficient for the mass of activated carbon used to fix onto the titanium current collector surfaces. Therefore, the electrode material tends to peel off, giving an inferior performance. When the binder used is too much, the electronic conductivity of the activated carbon electrode material decreases. This effect tends to increase the shunt resistance of the device, again reducing the performance of the supercapacitor fabricated. Therefore, the optimum performance of the supercapacitor is obtained when the PVP binder used is 5 % m/m of the activated carbon used in making the suspension for fabricating electrodes.

The specific capacitance depends on the performance of the electrode materials in addition to those of the electrolyte. The performance of electrode materials depends on the extent to which they are bound to the current collector surface, the porosity of the layer, the number of

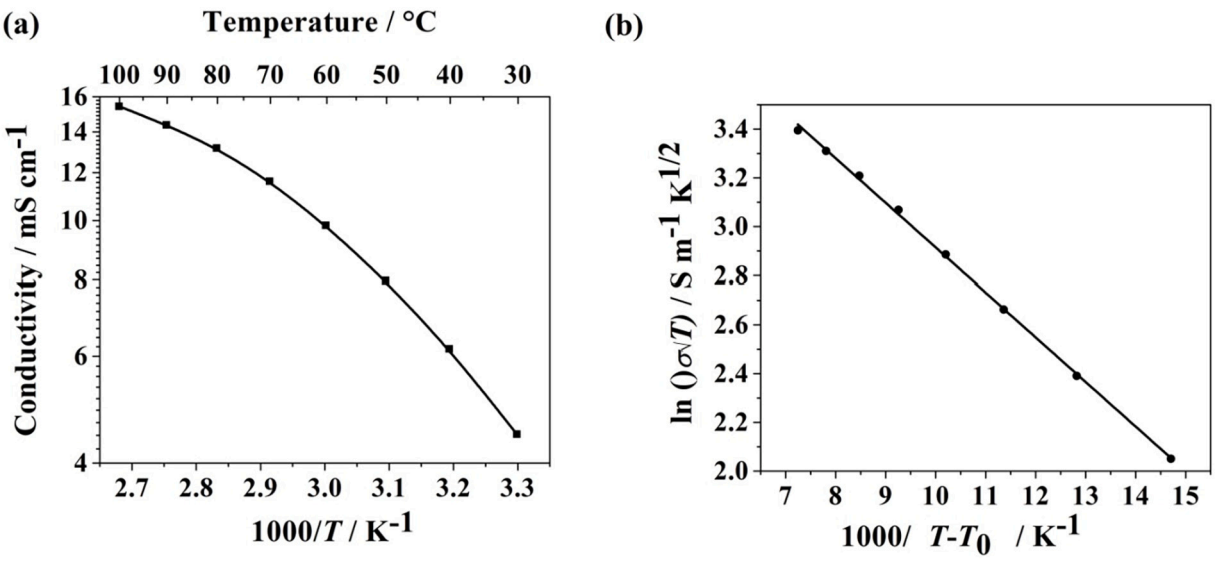

Fig. 6. (a) the Arrhenius and (b) Vogel-Tammann-Fulcher (VTF) plots for the temperature dependence of ionic conductivity of the trimethylammonium thiocyanate ionic liquid electrolyte.

Table 2
Specific capacitances of the supercapacitors made with different amounts of the polyvinylpyrrolidone binder in the 0.50 g activated carbon layer at 300 °C; cyclic voltammetry performed at 10 mV s^{-1} scan rate.

Cell No.	Binder%	Area under the CV curve (V A)	C_m (F g^{-1})
1	2	0.0059	18.4
2	5	0.0068	28.3
3	7	0.0023	23.0
4	10	0.0021	21.4
5	15	0.0031	19.4

active sites available, and the electronic conductivity of the electrode material used. These properties depend on the parameters used in the fabrication of the electrode material. Since the best performance is observed for cell No. 2, which comprised 0.50 g of activated carbon with 5 % PVP binder used in the preparation of the electrode material, this cell was used for the investigation of the specific capacitance of the supercapacitor fabricated using the electrodes fabricated at different temperatures from 100 °C to 300 °C. Table 3 depicts the data obtained. As can be observed from the data given in Table 3, the specific capacitance of the supercapacitor increases when the temperature of the electrode is increased from 100 °C to 200 °C beyond which it progressively decreases. This is possible since the temperature increases, the binding of the electrode material to the current collector surface becomes better, thus giving rise to lowered electrical resistance between the current collector/electrode material junction. However, when the temperature is increased beyond 250 °C, the PVP binder tends to burn, thus causing poor adhesion of the electrode material to the current collector surface. As a result of this, the resistance at the junction increases. The maximum specific capacitance of 33.47 F g^{-1} is obtained at the optimum temperature of 200 °C, at which electrodes were fabricated.

Table 3
Specific capacitance of the supercapacitor cell No. 2 at different temperatures; cyclic voltammetry performed at 10 mV s^{-1} scan rate.

T (°C)	Area under the CV curve (V A)	Cm (F g^{-1})
100	0.0043	17.70
150	0.0021	20.95
200	0.0027	33.47
250	0.0070	29.30
300	0.0077	24.00
350	0.0041	20.50

3.4. Electrochemical characterizations

3.4.1. Cyclic voltammetry (CV) characteristics

Fig. 7 shows the CV characteristics of the TAT-based supercapacitor, at different scan rates, with optimized amounts of activated carbon and binder composition (5 % m/m) used in fabricating electrodes, which were treated at the optimized temperature of 200 °C that gave the highest specific capacitance. The specific capacitance data calculated at different scan rates are given in Table 4. As shown in Eq. (2), the increase in the scan rate, $\frac{dV}{dt}$, tends to decrease the specific capacitance, *C*, and the behavior is confirmed by the CVs given in Fig. 7(a) and the data shown in Table 4.

In Fig. 7(a), the rectangular shapes of the CVs and the absence of any redox peaks in CVs measured at different scan rates illustrate the electric double layer capacitance behavior of the SCs [36]. Aqueous acid or base type electrolytes (H_2SO_4, KOH) have higher conductivities (up to 1 S cm^{-1}) than those of organic/ionic electrolytes, but the operating voltage is relatively low (below 1.1 V) due to water's low electrochemical stability window (1.23 V) [37]. Fig. 7 (b) shows seven CV curves for the cell containing TAT ionic liquid electrolyte in different OPWS between 0 and 1 and 0–2.2 V at a scan rate of 10 mV s^{-1}. As shown in Fig. 7 (b), when the voltage exceeds 2.0 V, the CV rectangular shape of the curves is distorted, but no traces of side reactions were observed. Above 2.0 V, the current increases quickly, which indicates the presence of a Faradic reaction in the electrolyte [38]. However, as shown in Fig. 7 (b), 1.8 V is a suitable operating voltage for the TAT electrolyte.

3.4.2. Capacitive and diffusive analysis

CV curves (Fig. 7 (a)) are further analyzed to determine the contribution of capacitive and diffusive control processes to current density. Eq. (6) illustrates the contribution of capacitive and diffusive control process current to total current [39–41].

$$i(v) = k_1 v + k_2 v^{0.5} \quad (6)$$

where, $i(v)$ is the current response at a specific voltage, v is the scan rate, and k_1 & k_2 are constants. Here, the $k_1 v$ term relates to the capacitive current and the $k_2 v^{0.5}$ term relates to the diffusive current [39]. Fig. 8

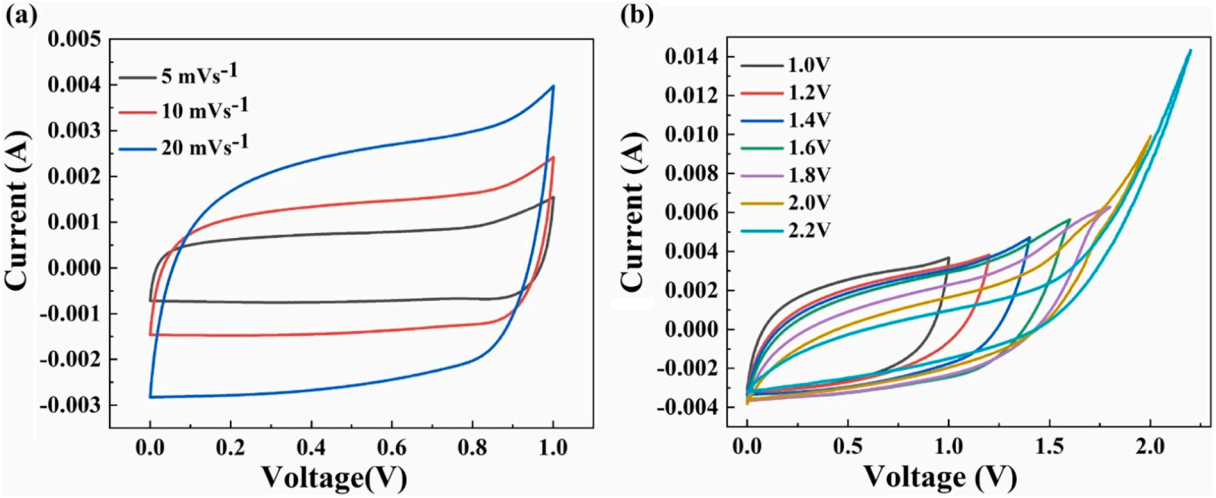

Fig. 7. (a) The cyclic voltammograms, recorded at different scan rates, 5, 10, and 15 mV s^{-1}, of the supercapacitor made with the optimized dosage of the electrode materials treated at the optimized temperature of 200 °C and (b) cyclic volumetric curves of the cell for different operating voltage windows at scan rate 10 mV s^{-1}.

Table 4
The specific capacitance data obtained from cyclic voltammograms recorded at three scan rates.

Mass of activated material deposited on Titanium plate ($\times 10^{-3}$ g)	Potential scan rate (mV s^{1})	Area under CV curve (V A)	Specific capacitance (F g^{-1})
4.00	5	0.00147	36.8
4.00	10	0.00267	33.5
4.00	20	0.00472	29.5

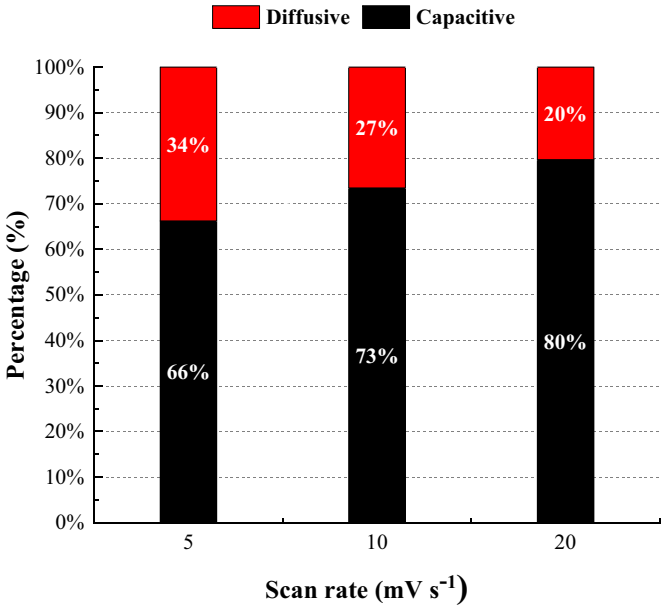

Fig. 8. Capacitive and diffusive contributions to the total current at different scan rates.

depicts the diffusive and capacitive behavior of a TAT supercapacitor at different scan rates. The diffusive contribution decreases from 34 % to 20 % with an increase in scan rate. This implies that there is no sufficient time to transport ions into electrodes at faster scan rates. The scan rate doesn't seem to have any impact on the capacitive element.

3.4.3. Galvanostatic charge/discharge (GCD) characteristics

The GCD curves measured under different current density ranges of 0.5, 1.0, 1.5, and 2.0 A g^{-1} are shown in Fig. 9, which depicts a nearly triangular shape and relatively fast current response that corresponds to double-layer capacitive behavior [38]. During the charging and discharging stages, a small sharp initial jump/drop in voltage is observed, which relates to the internal resistance, ESR, of the cell [42].

3.4.4. Electrochemical impedance spectroscopy (EIS) characteristics

To determine the behavior of supercapacitor, it is important to investigate the electrochemical impedance spectroscopic (EIS) data in a wide frequency range. Fig. 10 shows the Nyquist plot for the optimized cell and the inset shows the equivalent circuit used to fit data. The ion diffusion process within the AC electrode can be understood by electrochemical EIS data. The Nyquist plots show a relatively vertical spike in the low-frequency region, indicating the primary contribution of electrostatic ion adsorption and low diffusion resistance [36]. In addition, the low charge transfer resistance can be inferred from the small semicircle in the high-frequency region.

The X-axis intercept indicates the bulk or series resistance, R_s that

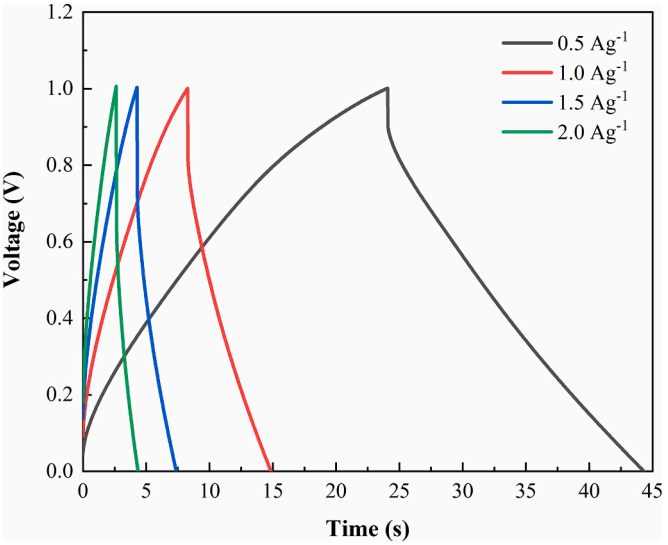

Fig. 9. The charge-discharge curves of the optimized supercapacitor measured at different current densities.

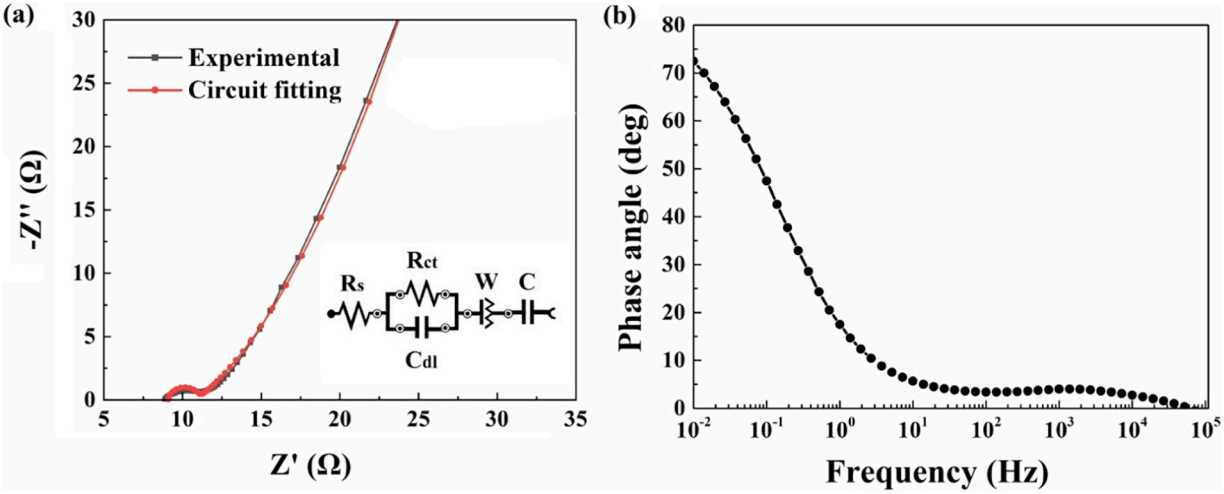

Fig. 10. (a) The Nyquist plot and (b) the phase angle versus frequency Bode plot for the optimized supercapacitor. The equivalent circuit used to fit the Nyquist plot is shown in the inset in Fig. 8. (a).

appears in the highest frequency range. It follows a semicircle part appearing in the next highest frequency range of 1 MHz to 0.5 MHz. The semicircle is caused by a parallel combination of charge transfer resistance and capacitance, R_{ct}, and the double layer capacitance C_{dl}. This indicates that Faradic reactions are occurring in the supercapacitor due to electro-active functional groups. It is implied in the curvature obtained in the linearly decreasing phase angle with log(frequency) in the Bode plot. It then follows a linear portion of approximately 45° inclination known as the Warburg impedance, *W*, and is caused by the ionic transport. The typical nearly constant phase angle demonstrated in the Bode plot also accounts for this constant phase element used in the equivalent circuit. At low frequencies, the electrodes' capacitance is increased due to a greater number of ions moving, resulting in a decrease in the capacitor's bulk resistance, which is typical of capacitive behavior with a capacitance C. The fitted data reveals R_s, R_{ct}, C_{dl}, W, and C are 9.09 Ω, 1.81 Ω, 57.3 μF, 81.3 mMho, and 127 mF, respectively. The bulk (series) resistance value obtained is comparable to that obtained for the electrolyte sandwiched between two stainless steel plates, as shown in the data given in Table 1. The much lower charge transfer resistance and typical double-layer capacitance in μF show that the Faradic reactions occurring are fast. The mMho range of Warburg impedance indicates fast ion transport within the electrolyte and within the pores of the electrode material. The capacitance of the supercapacitor, 127 mF, when divided by the mass of the electrode material, 4.0 mg, gives the specific capacitance to be 28.0 F g^{-1} and is comparable to that obtained from GCD experiments (29.6–36.8 F g^{-1}). Therefore, the independent methods used to determine the specific capacitance of the optimized supercapacitor give reasonably close results indicating that the data obtained are acceptable with a small error margin.

The cycle life of a supercapacitor is a significant factor to consider when dealing with real-world applications. To analyze the cell's electrochemical stability, 1000 CV cycles were performed (Fig. 11. (a)). The specific capacitance of a supercapacitor with TAT electrolyte as a function of cycle number is shown in Fig. 11. (b).

Fig. 11. (a) shows the cyclic voltammograms of the optimized supercapacitor measured at a scan rate of 100 mV s^{-1} for 1000 cycles. Only the curves for every 100 cycles are shown since the curves were crowded. In addition, two Nyquist plots were obtained before and after 1000 cycles to evaluate the changes that happened to the supercapacitor during the continuous CV experiment. Fig. 12 shows the impedance curves taken before and after taking 1000 CV curves. After 1000 cycles, the Nyquist plot has shifted to the left side, indicating the reduction of the resistance of the electrode and the electrolyte. This small shift can be due to the slight increase in temperature. In other words, the ESR value appears to be slightly lower than its initial value, indicating that the internal resistance of the cell has decreased. This drop in resistance may

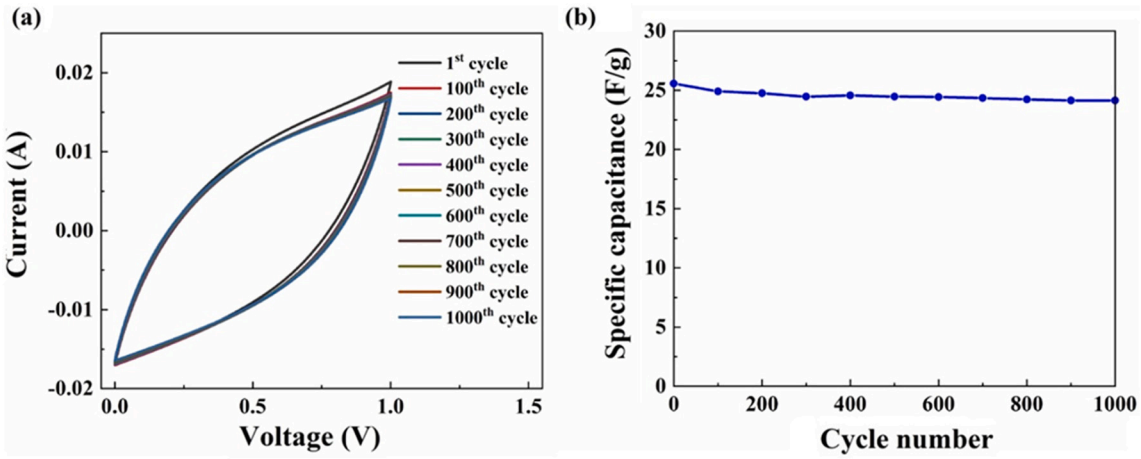

Fig. 11. (a) The cyclic voltammograms of optimized supercapacitor with TAT electrolyte at scan rate 100 mV s^{-1} for 1000 cycles (curves are shown for each 100 cyclic) (b) cycling performance of the optimized supercapacitor for 1000 cycles (calculation were conducted for 100 steps).

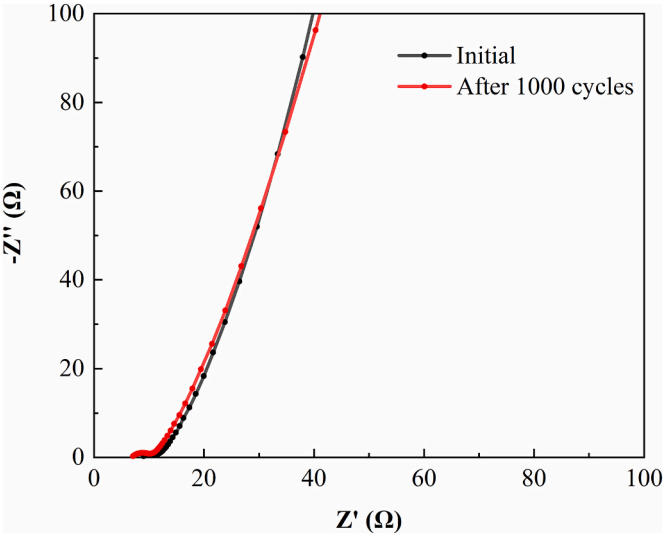

Fig. 12. The Nyquist plot of supercapacitor with triethylammonium thiocyanate electrolyte after 0 and 1000 cycles.

be due to the slight increase in temperature caused by the conduction of large number of cycles continuously and the improved charge transport between electrode and electrolyte.

The initial specific capacitance was 25.6 F g^{-1}, but after continuing 1000 cycles, it decreased slightly to reach 24.1 F g^{-1} The results indicate that the TAT-based supercapacitor exhibits extremely good capacity retention of 94.4 %, which is indicative of the high stability of the ionic liquid and activated carbon. The specific capacitance against cycle number is shown in Fig. 11. (b) which also indicates the high stability of the device as well as the components.

4. Conclusion

In conclusion, we made an activated charcoal supercapacitor with polyvinylpyrrolidone (PVP) electrodes and trimethylammonium thiocyanate (TAT) ionic liquid as the electrolyte. This supercapacitor electrolyte performs exceptionally well, and this is the first time the activated carbon/polyvinylpyrrolidone binder/triethylammonium thiocyanate ionic liquid electrolyte combination-based supercapacitors were fabricated and characterized. The sintering temperatures of activated carbon and PVP electrodes, as well as the binder quantity percentage in activated carbon electrodes, were investigated. The optimal binder percentage is 5 % of activated carbon quantity, and the specific capacitance of the supercapacitor is 36.8 F $g^{-1}$when the electrodes are sintered at 200 °C for 20 min. The supercapacitor has been characterized using a variety of approaches, and these observations have been shown to be in good agreement with each other.

Furthermore, after 1000 cycles, the TAT-based supercapacitor showed good electrochemical stability, with 94.4 % capacity retention. The results reveal that TAT ionic electrolyte can successfully be used in supercapacitor applications, which would eliminate the drawbacks of aqueous electrolytes. There seem to be Faradic reactions due to electroactive functional groups present on the activated carbon surface. These functional groups have to be removed to minimize such undesired side reactions.

Declaration of competing interest

The authors declare that they have no known competing financial interests or personal relationships that could have appeared to influence the work reported in this paper.

Data availability

Data will be made available on request.

References

[1] S. Shafiee, E. Topal, When will fossil fuel reserves be diminished? Energy Policy 37 (2009) 181–189, https://doi.org/10.1016/j.enpol.2008.08.016.
[2] Y. Nishi, Lithium ion secondary batteries; past 10 years and the future, J. Power Sources 100 (2001) 101–106, https://doi.org/10.1016/S0378-7753(01)00887-4.
[3] U. Lucia, Overview on fuel cells, Renew. Sust. Energ. Rev. 30 (2014) 164–169, https://doi.org/10.1016/j.rser.2013.09.025.
[4] P. Simon, Y. Gogotsi, Charge storage mechanism in nanoporous carbons and its consequence for electrical double layer capacitors, Philos. Trans. R. Soc. A Math. Phys. Eng. Sci. 368 (2010) 3457–3467, https://doi.org/10.1098/rsta.2010.0109.
[5] G.Z. Chen, Understanding supercapacitors based on nano-hybrid materials with interfacial conjugation, Prog. Nat. Sci. Mater. Int. 23 (2013) 245–255, https://doi.org/10.1016/j.pnsc.2013.04.001.
[6] A. Shajkumar, S. Sahu, N. Duraisamy, L. Schmidt-Mende, A. Ramadoss, Layered double hydroxide as electrode material for high-performance supercapattery, in: Adv. Supercapacitor Supercapattery, Elsevier, 2021, pp. 199–254, https://doi.org/10.1016/b978-0-12-819897-1.00011-2.
[7] J.R. Miller, A.F. Burke, Electrochemical capacitors: challenges and opportunities for real-world applications, Electrochem. Soc. Interface 17 (2008) 53–57, https://doi.org/10.1149/2.F08081IF/XML.
[8] K. Li, P. Li, Z. Sun, J. Shi, M. Huang, J. Chen, S. Liu, Z. Shi, H. Wang, All-cellulose-based quasi-solid-state supercapacitor with nitrogen and boron dual-doped carbon electrodes exhibiting high energy density and excellent cyclic stability, Green Energy Environ. (2022), https://doi.org/10.1016/J.GEE.2022.01.002.
[9] Z. Zhu, S. Tang, J. Yuan, X. Qin, Y. Deng, R. Qu, G.M. Haarberg, Effects of various binders on supercapacitor performances, Int. J. Electrochem. Sci. 11 (2016) 8270–8279, https://doi.org/10.20964/2016.10.04.
[10] X.Z. Sun, X. Zhang, B. Huang, Y.W. Ma, Effects of separator on the electrochemical performance of electrical double-layer capacitor and hybrid battery-supercapacitor, wuli huaxue Xuebao/, Acta Phys. - Chim. Sin. 30 (2014) 485–491, https://doi.org/10.3866/PKU.WHXB201401131.
[11] J. Zhu, Y. Xu, J. Wang, J. Lin, X. Sun, S. Mao, The effect of various electrolyte cations on electrochemical performance of polypyrrole/RGO based supercapacitors, Phys. Chem. Chem. Phys. 17 (2015) 28666–28673, https://doi.org/10.1039/C5CP04080A.
[12] M. Arulepp, L. Permann, J. Leis, A. Perkson, K. Rumma, A. Jänes, E. Lust, Influence of the solvent properties on the characteristics of a double layer capacitor, J. Power Sources 133 (2004) 320–328, https://doi.org/10.1016/J.JPOWSOUR.2004.03.026.
[13] N.M. Keppetipola, M. Dissanayake, P. Dissanayake, B. Karunarathne, M. A. Dourges, D. Talaga, L. Servant, C. Olivier, T. Toupance, S. Uchida, K. Tennakone, G.R.A. Kumara, L. Cojocaru, Graphite-type activated carbon from coconut shell: a natural source for eco-friendly non-volatile storage devices, RSC Adv. 11 (2021) 2854–2865, https://doi.org/10.1039/D0RA09182K.
[14] K.V.G. Raghavendra, R. Vinoth, K. Zeb, C.V.V. Muralee Gopi, S. Sambasivam, M. R. Kummara, I.M. Obaidat, H.J. Kim, An intuitive review of supercapacitors with recent progress and novel device applications, J. Energy Storage 31 (2020), 101652, https://doi.org/10.1016/j.est.2020.101652.
[15] S. Makino, Y. Yamauchi, W. Sugimoto, Synthesis of electro-deposited ordered mesoporous RuOx using lyotropic liquid crystal and application toward micro-supercapacitors, J. Power Sources 227 (2013) 153–160, https://doi.org/10.1016/J.JPOWSOUR.2012.11.032.
[16] J.S. Lee, S.I. Kim, J.C. Yoon, J.H. Jang, Chemical vapor deposition of mesoporous graphene nanoballs for supercapacitor, ACS Nano 7 (2013) 6047–6055, https://doi.org/10.1021/NN401850Z/SUPPL_FILE/NN401850Z_SI_001.PDF.
[17] S. Zhang, Y. Li, N. Pan, Graphene based supercapacitor fabricated by vacuum filtration deposition, J. Power Sources 206 (2012) 476–482, https://doi.org/10.1016/J.JPOWSOUR.2012.01.124.
[18] O. Ibukun, H.K. Jeong, Effects of aqueous electrolytes in supercapacitors, New Phys. Sae Mulli. 69 (2019) 154–158, https://doi.org/10.3938/NPSM.69.154.
[19] M. Aslan, D. Weingarth, N. Jäckel, J.S. Atchison, I. Grobelsek, V. Presser, Polyvinylpyrrolidone as binder for castable supercapacitor electrodes with high electrochemical performance in organic electrolytes, J. Power Sources 266 (2014) 374–383, https://doi.org/10.1016/J.JPOWSOUR.2014.05.031.
[20] K.L. Van Aken, M. Beidaghi, Y. Gogotsi, Formulation of ionic-liquid electrolyte to expand the voltage window of supercapacitors, Angew. Chem. 127 (2015) 4888–4891, https://doi.org/10.1002/ANGE.201412257.
[21] K. Naoi, "Nanohybrid capacitor": the next generation electrochemical capacitors, Fuel Cells 10 (2010) 825–833, https://doi.org/10.1002/FUCE.201000041.
[22] A. Oz, D. Gelman, E. Goren, N. Shomrat, S. Baltianski, Y. Tsur, A novel approach for supercapacitors degradation characterization, J. Power Sources 355 (2017) 74–82, https://doi.org/10.1016/J.JPOWSOUR.2017.04.048.
[23] A.G. Pandolfo, A.F. Hollenkamp, Carbon properties and their role in supercapacitors, J. Power Sources 157 (2006) 11–27, https://doi.org/10.1016/J.JPOWSOUR.2006.02.065.
[24] G.R.A. Kumara, S. Kaneko, M. Okuya, K. Tennakone, Fabrication of dye-sensitized solar cells using triethylamine hydrothiocyanate as a CuI crystal growth inhibitor, Langmuir 18 (2002) 10493–10495, https://doi.org/10.1021/LA020421P.

[25] H.J. Kim, T.N.V. Krishna, K. Zeb, V. Rajangam, C.V.V.Muralee Gopi, S. Sambasivam, K.V.G. Raghavendra, I.M. Obaidat, A comprehensive review of Li-ion battery materials and their recycling techniques, Electron 9 (2020) 1161, https://doi.org/10.3390/ELECTRONICS9071161, 9 (2020) 1161.
[26] E. Frackowiak, S. Delpeux, K. Jurewicz, K. Szostak, D. Cazorla-Amoros, F. Béguin, Enhanced capacitance of carbon nanotubes through chemical activation, Chem. Phys. Lett. 361 (2002) 35–41, https://doi.org/10.1016/S0009-2614(02)00684-X.
[27] C. Long, L. Jiang, X. Wu, Y. Jiang, D. Yang, C. Wang, T. Wei, Z. Fan, Facile synthesis of functionalized porous carbon with three-dimensional interconnected pore structure for high volumetric performance supercapacitors, Carbon N. Y. 93 (2015) 412–420, https://doi.org/10.1016/J.CARBON.2015.05.040.
[28] J. Gamby, P.L. Taberna, P. Simon, J.F. Fauvarque, M. Chesneau, Studies and characterisations of various activated carbons used for carbon/carbon supercapacitors, J. Power Sources 101 (2001) 109–116, https://doi.org/10.1016/S0378-7753(01)00707-8.
[29] C. Vix-Guterl, S. Saadallah, K. Jurewicz, E. Frackowiak, M. Reda, J. Parmentier, J. Patarin, F. Beguin, Supercapacitor electrodes from new ordered porous carbon materials obtained by a templating procedure, Mater. Sci. Eng. B 108 (2004) 148–155, https://doi.org/10.1016/J.MSEB.2003.10.096.
[30] D. A, S.A.B.A. Manaf, G. Hegde, Low cost, high performance supercapacitor electrode using coconut wastes: eco-friendly approach, J. Energy Chem. 25 (2016) 880–887, https://doi.org/10.1016/J.JECHEM.2016.08.002.
[31] J. Li, X. Wang, Q. Huang, S. Gamboa, P.J. Sebastian, Studies on preparation and performances of carbon aerogel electrodes for the application of supercapacitor, J. Power Sources 158 (2006) 784–788, https://doi.org/10.1016/J.JPOWSOUR.2005.09.045.
[32] A. Konno, T. Kitagawa, D. Sugiura, G.R.A. Kumara, K. Tennakone, The effect of room temperature molten thiocyanate salts in CuI on the performance of solid-state dye-sensitized photovoltaic cells using CuI as a hole collector, in: Proc. - Electrochem. Soc, 2004, pp. 213–216. https://www.researchgate.net/publication/287021245_The_effect_of_room_temperature_molten_thiocyanate_salts_in_CuI_on_the_performance_of_solid-state_dye-sensitized_photovoltaic_cells_using_CuI_as_a_hole_collector. (Accessed 6 January 2022).
[33] E. Fazio, M. Latino, F. Neri, F. Bonsignore, in: Raman Scattering Study of Evaporated Carbon Nanostructured Films, 2008, pp. 153–156, doi:10.1002/jrs.
[34] A. Cuesta, P. Dhamelincourt, J. Laureyns, A. Martínez-Alonso, J.M.D. Tascón, Raman microprobe studies on carbon materials, Carbon N. Y. 32 (1994) 1523–1532, https://doi.org/10.1016/0008-6223(94)90148-1.
[35] Y. Okada, M. Ikeda, M. Aniya, Non-arrhenius ionic conductivity in solid electrolytes: a theoretical model and its relation with the bonding nature, Solid State Ionics 281 (2015) 43–48, https://doi.org/10.1016/j.ssi.2015.08.020.
[36] R. Vinodh, C.V.V.M. Gopi, V.G.R. Kummara, R. Atchudan, T. Ahamad, S. Sambasivam, M. Yi, I.M. Obaidat, H.J. Kim, A review on porous carbon electrode material derived from hypercross-linked polymers for supercapacitor applications, J. Energy Storage 32 (2020), 101831, https://doi.org/10.1016/J.EST.2020.101831.
[37] A. Burke, R&D considerations for the performance and application of electrochemical capacitors, Electrochim. Acta 53 (2007) 1083–1091, https://doi.org/10.1016/J.ELECTACTA.2007.01.011.
[38] S. Vaquero, J. Palma, M. Anderson, R. Marcilla, Mass-balancing of electrodes as a strategy to widen the operating voltage window of carbon/carbon supercapacitors in neutral aqueous electrolytes, Int. J. Electrochem. Sci. 8 (2013) 10293–10307.
[39] M.Z. Iqbal, M.M. Faisal, M. Sulman, S.R. Ali, A.M. Afzal, M.A. Kamran, T. Alharbi, Capacitive and diffusive contribution in strontium phosphide-polyaniline based supercapattery, J. Energy Storage 29 (2020), 101324, https://doi.org/10.1016/J.EST.2020.101324.
[40] T. Brezesinski, J. Wang, J. Polleux, B. Dunn, S.H. Tolbert, Templated nanocrystal-based porous TiO2 films for next-generation electrochemical capacitors, J. Am. Chem. Soc. 131 (2009) 1802–1809, https://doi.org/10.1021/JA8057309/SUPPL_FILE/JA8057309_SI_001.PDF.
[41] T.-C. Liu, W.G. Pell, B.E. Conway, S.L. Roberson, Behavior of molybdenum nitrides as materials for electrochemical capacitors: comparison with ruthenium oxide, J. Electrochem. Soc. 145 (1998) 1882–1888, https://doi.org/10.1149/1.1838571/XML.
[42] G.P. Pandey, A.C. Rastogi, Graphene-based all-solid-state supercapacitor with ionic liquid gel polymer electrolyte, MRS Online Proc.Libr. 14401 (1440) (2012) 25–30, https://doi.org/10.1557/OPL.2012.1279, 2012.